

# Modeling Study of Neopentane Oxidation in a Pressurized Flow Reactor at 8 Atmospheres.

Suqing Wang, David L. Miller, and Nicholas P. Cernansky

*Department of Mechanical Engineering and Mechanics, Drexel University, PA 19104.*

Henry J. Curran, William J. Pitz and Charles K. Westbrook

*Lawrence Livermore National Laboratory, Livermore, CA 94551.*

## Abstract

An existing detailed chemical kinetic reaction mechanism for neopentane oxidation [1] is applied to new experimental measurements taken in a flow reactor [2] operating at a pressure of 8 atm. The reactor temperature ranged from 620 K to 810 K and flow rates of the reactant gases neopentane, oxygen, and nitrogen were 0.285, 7.6 and 137.1 standard liter per minute (SLM), respectively, producing an equivalence ratio of 0.3. Initial simulations identified some deficiencies in the existing model and the paper presents modifications which included upgrading the thermodynamic parameters of alkyl radical and alkylperoxy radical species, adding an alternative isomerization reaction of hydroperoxy-neopentyl-peroxy and a multi-step reaction sequence for 2-methylpropan-2-yl radical with molecular oxygen. These changes improved the calculation for the overall reactivity and the concentration profiles of the following primary products: formaldehyde, acetone, isobutene, 3,3-dimethyloxetane, methacrolein, carbon monoxide, carbon dioxide and water. Experiments indicate that neopentane shows negative temperature coefficient behavior similar to other alkanes, though it is not as pronounced as that shown by n-pentane for example. Modeling results indicate that this behavior is caused by the  $\beta$ -scission of the neopentyl radical and the chain propagation reactions of the hydroperoxyl-neopentyl radical.

## Full-length article

Corresponding Author: Dr. Henry J. Curran  
L-370,  
Lawrence Livermore National Laboratory,  
Livermore, CA 94551  
Phone: (925)-422-5790  
Fax: (925)-423-0909  
e-mail: curran6@llnl.gov

## Introduction

Preignition of hydrocarbons has been studied in internal combustion engines [3, 4, 5]. However, the detailed mechanism of preignition chemistry, under relevant conditions ( $T \ll 1000$  K,  $P > 1$  atm), is not well understood. In view of this, we have developed a program to investigate the detailed kinetic mechanism of hydrocarbons under these conditions.

Neopentane, because to its unique molecular structure, i.e. all hydrogen atoms are equivalent with only one parent alkyl radical *via* H atom abstraction, has been the subject of several oxidation studies [6, 7, 8, 9, 10]. In addition, neopentane does not form a  $C_5$  conjugate olefin from its hydroperoxy-alkyl radical. Conjugate olefins have been identified as controlling intermediates in the preignition process of hydrocarbons. Specifically, formation of the conjugate olefin is considered the key step in the unique phenomenon of low and intermediate temperature hydrocarbon oxidation called negative temperature coefficient (NTC) behavior. During the transition from low to intermediate temperature oxidation, the overall reactivity of the hydrocarbon oxidation decreases as reaction temperature increases. In previous neopentane oxidation experiments [6, 11] cool flames of neopentane were observed, implying that neopentane oxidation should also exhibit NTC behavior. In the recent experimental study of neopentane oxidation at Drexel University using a pressurized flow reactor [2], NTC behavior has been confirmed.

In our previous detailed modeling study [1], an intermediate temperature oxidation mechanism for the combustion of neopentane was developed and compared to the experimental results of Baker et al. [9, 10]. The detailed model matched both primary and secondary products measured in those studies. However, the experiments covered a limited range of conditions: (1) the reaction temperature was constant at 753 K and (2) the pressure was subatmospheric at 0.65 atm. In the present work, simulations using the detailed neopentane oxidation mechanism will be compared to new experimental data with the purpose of extending the range of applicability of the model.

## Experimental

The neopentane oxidation experiments were conducted in the Drexel University pressurized flow reactor. The facility and experimental techniques have been described elsewhere [12, 13]. Neopentane used in the experiments was supplied by Quality Standard and Research Gases with purity of more than 97%. The two primary impurities are n-butane and iso-pentane. Since the typical products from n-butane and iso-pentane oxidation, such as 1-butene and pentene, were not observed in the experiments, the effects of these impurities were assumed negligible. Liquid nitrogen and gaseous oxygen were from BOC Gases with purity more than 99.6%. Neopentane was metered in the liquid phase through a calibrated capillary tube with the flow monitored and controlled using a differential pressure transducer and computer controlled metering valve, respectively. Before neopentane enters the reactor, it merges with heated nitrogen and evaporates. The reactor pressure is controlled by a stainless steel regulating valve near the exhaust and is measured by two pressure transducers at the entrance and exit of the reactor. Neopentane has a boiling point of 9.5 °C at 1 atm and 86 °C at 8 atm. The flow rate is controlled in the liquid phase. However, neopentane evaporates before it enters the mixing nozzle, where the temperature is greater than 500 K, and thus significantly higher than the boiling point of the fuel. The evaporated neopentane is forced out through six fuel nozzles into the narrow annulus just downstream of the  $O_2/N_2$  mixture

jets. The high level of turbulence, induced by the opposing jets of fuel and  $O_2/N_2$  mixture stream, provides a region of rapid mixing and ensures that the fuel is well mixed with the  $O_2/N_2$  mixture.

In these experiments, nitrogen and oxygen were mixed together to obtain a synthetic air mixture free of carbon dioxide and the equivalence ratio was calculated with this synthetic air. Additional nitrogen was added to dilute the mixture and to minimize the temperature rise due to exothermicity. The dilution is defined in terms of volumetric flow rates of air and nitrogen:  $V(N_2)/(V(\text{air}) + V(N_2))$ . The equivalence ratio was maintained at 0.3 in all experiments while different dilutions can be obtained by changing the  $N_2$ ,  $O_2$  and fuel flow rates. In this study, a dilution of 75% was maintained. The flow rate of neopentane was calibrated just before running the experiments. To do this, we first substituted the required flow rate of  $O_2$  with  $N_2$ , so that there was no reaction during the calibration. Then, we used a differential pressure transducer and a computer controlled step motor to control the opening of the needle valve in the flow line. The voltage output from the differential pressure transducer varies proportionally to the change in liquid fuel flow rate. After the reactor system was stabilized under the experimental condition, the samples (mixture of  $N_2$  and neopentane vapor) inside the reactor were directed to the FTIR where the concentration of neopentane was measured. When the concentration of neopentane reached the desired value, the corresponding voltage output from the differential pressure transducer was sent to the computer as the baseline. The Labview controlled program then automatically drove the step motor to control the needle valve and maintain a constant fuel flow rate. The concentration of the fuel was measured a second time and it was found that the error between the real concentration and the desired value to be less than 0.5%. (For the 75%  $N_2$  dilution case, the real concentration of neopentane was 1960 ppm while the desired value was 1966 ppm. For 85%  $N_2$  dilution case, they were 1215 ppm and 1220 ppm, respectively.)

A glass-lined hot water cooled gas sampling probe with thermocouple is mounted on a computer-controlled translating table, which moves the probe along the reactor center-line to extract gas samples at selected locations. The extracted sample is split with some sample flowing to an on-line non-dispersive infrared analyzer to measure carbon monoxide (CO) and the rest directed to an optical cell for Fourier transform infrared (FTIR) species analysis. FTIR takes the absorbance spectra as a function of wavenumber for samples (exhaust mixture from neopentane oxidation) collected in an optical cell. According to Beer's law, the absorbance of overall spectra is the linear addition of those of pure species, while each species also has its own featured spectra, i.e. absorbance at different wavenumbers. Therefore, the spectra are compared with a built-in standard known infrared spectra library. The SEARCH software [14]–[17] can identify species in the compound based on Hit Quality Index (HQI). (note: FTIR does not involve any physical separation, such as occurs in the column of a GC system.) In addition, we have generated a set of standard spectra of possible species with known concentrations. To quantify the species, we used the subtraction method of FTIR systems. The library contains spectra of identified pure species in known concentrations. These spectra are multiplied by a multiplication factor and subtracted in sequence from the overall spectra. The multiplication factor can be used to calculate the concentration of specific species in the sample. After subtracting all of the identified species in the sample spectra, the remaining absorbance spectra becomes a fairly flat line, indicating we have identified and quantified the species. For example, if the spectra of a species, which

does not exist in the sample, is subtracted from sample spectra, there will be a valley in the remaining spectra. On the other hand, if the spectra of a species, which does exist in the compound, is not subtracted from sample spectra, there will be a peak in the remaining spectra. In addition, many compounds have absorbance peaks at different wavenumbers and thus can be easily identified using a library. For example, isobutene has a feature absorbance peak at  $890\text{ cm}^{-1}$  while 1-pentene has the feature absorbance at  $910\text{ cm}^{-1}$ . Therefore, it is easy to distinguish them using their FTIR spectra. For the same reason, acetone and 3,3-dimethyloxetane are positively identified. Acetone and 2-butanone have featured absorbance peak at  $1217\text{ cm}^{-1}$  and  $1741\text{ cm}^{-1}$ , respectively and thus one cannot be mistaken for the other. Among the species detected and quantified were neopentane, formaldehyde, acetone, isobutene, 3,3-dimethyloxetane, methacrolein, formic acid, carbon monoxide, carbon dioxide and water.

Two sets of experiments were used for the modeling study. All experiments were carried out at an equivalence ratio of 0.3, pressure of 8 atmospheres and 75% nitrogen dilution [2]. First, we conducted reactivity mapping experiments with a constant residence time (CRT) of 200 ms, and a nitrogen dilution of 85%. However, in order to facilitate the species measurements, the reactivity was promoted by reducing the nitrogen dilution to 75%. The reactor was heated to 810 K and after conditions stabilized, the heaters were turned off which causes the reactor to cool at a rate of  $2\text{--}5\text{ }^{\circ}\text{C}/\text{min}$ . As the reaction gases cool, the probe moves towards the inlet to maintain constant residence time at the sampling point. A series of sample FTIR spectra were taken for species measurement while CO formation was continuously monitored as an indication of overall reactivity. Figure 1 shows a comparison of CO production, used to characterize extent of reaction, at 75% and 85% nitrogen dilution in addition to the comparable reactivity of n-pentane [18]. Note that at 85% dilution, neopentane is much less reactive than n-pentane. Second, based on the observations from reactivity mapping experiments, we selected two reactor temperatures, 690 K and 757 K, for axial profiles at constant inlet temperature. The lower temperature is below the start of NTC and the higher one is in the NTC regime. Samples were taken at different positions along the reactor, which correspond to different residence times.

### Computational Model

Computer simulations were performed using the HCT code [19], which solves the coupled chemical kinetic and conservation equations for energy, mass and momentum under a variety of boundary and initial conditions for reactive systems. The high-pressure reactor experiments were simulated as an adiabatic, isobaric (8 atm) plug flow with negligible axial diffusion of species and energy. The detailed chemical kinetic reaction mechanism used in these calculations was based on previous work by the authors [1, 20, 21]. We employ the hierarchical nature of reacting systems starting with a core mechanism describing  $\text{H}_2/\text{O}_2$  and CO oxidation. To this is added the progressively larger  $\text{C}_1\text{--}\text{C}_4$  mechanism and ultimately the  $\text{C}_5$  neopentane mechanism whereby the complete model consists of approximately 390 different chemical species and 1875 elementary reactions.

In our more recent modeling work of neopentane oxidation [1] we have described the main reactions associated with the low-temperature portion of the mechanism. That mechanism has been applied to the current study but a number of changes have been made, and these are discussed below.

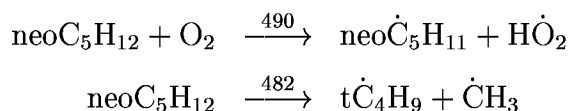
The thermodynamic properties for the relevant radicals and stable parent species were obtained by group additivity using THERM [22] with updated H/C/O groups and bond dissociation groups [23]. These thermochemical data allow calculation of reverse reaction rate constants by microscopic reversibility. We have updated the group values for alkyl-peroxide species based on the recent study of Lay and Bozzelli [24] and have modified these slightly so that the thermodynamic functions of  $\dot{\text{R}} + \text{O}_2 \rightleftharpoons \text{R}\dot{\text{O}}_2$  reactions agree with the experimental and calculated values of Knyazev and Slagle [25], Table 1. A comparison of our current THERM generated thermochemical values with those recommended by Knyazev and Slagle for a number of selected species are reported in Table 2. A listing of the thermodynamic parameters for the important species associated with neopentane oxidation are listed in Table 3, with the species names defined below. Our number for the heat of formation of the neopentyl radical is in good agreement with the values recommended by Slagle et al. [26] of  $8.735 \text{ kcal mol}^{-1}$ . Our entropy value for neopentyl radical is almost four units lower than  $83.34 \text{ cal mol}^{-1} \text{ K}^{-1}$  recommended by Slagle et al. but is in good agreement with that listed in the NIST structures and properties database, [27]. A full listing of the reaction mechanism can be obtained by Internet electronic mail (curran6@llnl.gov) or on disk by writing to the authors.

### Neopentane Oxidation

The overall reaction scheme for neopentane oxidation is depicted in Fig. 2. The species names are defined as follows:  $\text{neoC}_5\text{H}_{12}$  (neopentane),  $\text{neo}\dot{\text{C}}_5\text{H}_{11}$  (neopentyl radical),  $\text{iC}_4\text{H}_8$  (isobutene),  $\text{neoC}_5\text{H}_{11}\dot{\text{O}}_2$  (neopentyl-peroxy radical),  $\text{neo}\dot{\text{C}}_5\text{H}_{10}\text{OOH}$  (hydroperoxy-neopentyl radical),  $\text{neoC}_5\text{H}_{10}\text{O}$  (3,3-dimethyloxetane),  $\text{neoC}_5\text{H}_{10}\text{OOH}\cdot\dot{\text{O}}_2$  (hydroperoxy-neopentylperoxy radical),  $\text{iC}_4\text{H}_7\text{OOH}$  (isobutenyl-hydroperoxide),  $\text{neo}\dot{\text{C}}_5\text{H}_9\text{q}_2$  (dihydro-peroxide-neopentyl radical),  $\text{neoC}_5\text{ket}$  (2-methyl isopropanal-2-methylhydroperoxide),  $\text{neoC}_5\text{ketox}$  (2-methyl isopropanal-2-methoxy radical), and  $\text{neoC}_5\text{kejol}$  (3-hydroxy-2,2-dimethyl-propanal radical).

The present study was carried out in the temperature range 620–810 K, the region in which low temperature kinetics dominate. Low temperature oxidation of hydrocarbons has been discussed extensively in the literature [21, 28, 29, 30], so only the highlights relevant to neopentane oxidation will be discussed here. At low temperatures, chain branching is due primarily to the reaction pathway leading through 2-methyl isopropanal-2-methylhydroperoxide. From 620–690 K we observe increasing overall reactivity with increasing temperature, as seen from the decreasing neopentane concentrations in Fig. 6. As the temperature increases above 690 K the chain propagation reactions of the hydroperoxy-neopentyl species increase in importance, leading to the formation of heterocyclic species, olefins, and other  $\beta$ -decomposition products, Fig 5, with a corresponding decrease in the proportion of chain branching reactions. This competition, in addition to the  $\beta$ -scission of the neopentyl radical results in a gradual decrease in the overall reaction rate with increasing temperature a phenomenon known as negative temperature coefficient (NTC) behaviour.

In this study, initiation occurs mainly *via* H-atom abstraction by molecular oxygen with a small contribution from unimolecular fuel decomposition:



The numbers above the arrows refer to the reaction numbers in the kinetic mechanism. Initiation is followed by H-atom abstraction from the fuel, primarily by  $\dot{\text{O}}\text{H}$  radicals and to a lesser extent by  $\text{H}\dot{\text{O}}_2$ , and  $\dot{\text{O}}$  atoms. The neopentyl radical so produced, can either add to molecular oxygen producing neopentyl-peroxy radicals,  $\text{neoC}_5\text{H}_{11}\dot{\text{O}}_2$ , or undergo  $\beta$ -scission to give isobutene and methyl radicals. The rate of neopentyl radical addition to  $\text{O}_2$  was taken from Xi et al. [31] while the rate of neopentyl  $\beta$ -scission, reaction (493), was estimated in the reverse direction and calculated from microscopic reversibility. We choose to use our own estimate here as it best fits our data and is in good agreement with the value of Slagle and co-workers [26] in addition to the recommendations by Hughes et al. [32, 33], Baldwin et al. [34] and Tsang [35], Table 4.

Reactions of the  $\text{neoC}_5\text{H}_{11}\dot{\text{O}}_2$  species and the equilibrium of the  $\dot{\text{R}} + \text{O}_2 \rightleftharpoons \text{R}\dot{\text{O}}_2$  reaction are of great importance in determining both the product species distributions and the overall rate of fuel oxidation. There are three major types of reactions of the  $\text{neoC}_5\text{H}_{11}\dot{\text{O}}_2$  radicals.

1. Decomposition to  $\text{neo}\dot{\text{C}}_5\text{H}_{11} + \text{O}_2$ . This rate constant is calculated from the reverse rate constant and from the equilibrium constant (thermochemistry). Our equilibrium constant  $K_{\text{eq}}$  at 700 K for this reaction is  $2.17 \times 10^{-16} \text{ cm}^3 \text{ molecule}^{-1}$ , in contrast with  $3.89 \times 10^{-17} \text{ cm}^3 \text{ molecule}^{-1}$  recommended by Hughes et al. [32, 33]. This discrepancy of a factor of 5.6 is almost entirely due to the differences in the recommended enthalpies of reaction. We use -35.50 kcal/mol, while Hughes et al. measure -32.77 kcal/mol. At 700 K this difference is a factor of 7.0 which is very similar to difference in equilibrium constant expressions.
2. Intermolecular abstraction of hydrogen atoms from other hydrocarbon species to produce the stable neopentylhydroperoxide species,  $(\text{neoC}_5\text{H}_{11}\text{O}_2\text{H})$ , which then decomposes to  $\text{neoC}_5\text{H}_{11}\dot{\text{O}} + \dot{\text{O}}\text{H}$ , reaction (1320). The rate of this reaction is provided in Table 5 and is similar to that recommended by Sahetchian et al. [36] for various molecular hydroperoxide pyrolyses. The  $\text{neoC}_5\text{H}_{11}\dot{\text{O}}$  radical undergoes  $\beta$ -scission to yield formaldehyde and *tert*-butyl radical. Modeling results show that the reaction of  $\text{neoC}_5\text{H}_{11}\dot{\text{O}}_2$  with  $\text{H}\dot{\text{O}}_2$  radical is of some importance at lower temperatures (640–700 K). Our chosen rate constant is approximately a factor of two slower than the recommendation of Rowley et al. [37], reaction (1316), Table 5. The lower rate constant was chosen to get better agreement with the overall oxidation rate at lower temperatures. This reaction leads (indirectly) to the formation of significant quantities of acetone as indicated in our discussion below.
3. Isomerization of the neopentyl-peroxy radical *via* internal H-atom transfer to form a hydroperoxy-neopentyl radical,  $\text{neo}\dot{\text{C}}_5\text{H}_{10}\text{OOH}$ , reaction (1315). The rate of this isomerization has been a central issue in two studies; that of Baldwin et al. [34] at 753 K, and Hughes et al. [32, 33] in a flow system at 700 K. These studies both recognised the importance of the same isomerization reaction, and combined their experimental results with kinetic analyses to arrive at rates of this isomerization reaction at their respective temperatures. These rate expressions are summarized in Table 4 together with the rate constant we have used in our computations. All three rate expressions are evaluated at 700 K for the purpose of comparison. Our current rate expression is

about a factor of two faster than that recommended by Hughes et al. and Baldwin and co-workers.

In our present analysis of this reaction mechanism we calculate the forward isomerization rate constant based on the theoretical methods of Bozzelli [38], which has been described previously [21], and is based on our analysis of all possible  $\text{R}\dot{\text{O}}_2 \rightleftharpoons \dot{\text{Q}}\text{OOH}$  isomerizations presented in our n-heptane study [21]. The  $\mathcal{A}$ -factors for isomerization have been adjusted downwards to agree with a large number of comparisons between modeling and experimental results. The reverse isomerization rate constant is based on microscopic reversibility using calculated thermodynamic properties from THERM. Using these forward and reverse isomerization rate constants, the current model predicts rapid reaction in both directions with a net forward rate in good agreement with the rate constants reported by the experimental studies, Table 4. The experimental studies suggest a direct isomerization of neopentyl-peroxy radical to hydroperoxy-neopentyl radical with little or no reverse reaction, while reaction rates based on thermochemical analysis indicate a more rapid forward rate constant with significant reverse reaction.

The hydroperoxy-neopentyl radical formed can react *via* three major pathways.

1. Following Pollard [39], this species can react *via* O-O homolysis, producing the cyclic ether, 3,3-dimethyloxetane, and hydroxyl radical. The rate parameters for this reaction (1322) are given in Table 5 and are consistent with those reported in our earlier publication [1].
2. The  $\text{neo}\dot{\text{C}}_5\text{H}_{10}\text{OOH}$  species can undergo  $\beta$ -scission at two different sites, leading to the formation of two distinct sets of products. The hydroperoxy-neopentyl radical may scission to yield isobutene, formaldehyde and hydroxyl radical, reaction (1323), but can also lead to an alternative set of products, isobutenyl-hydroperoxide,  $\text{iC}_4\text{H}_7\text{OOH}$ , and methyl radical, reaction (1467). The rate for the formation of both sets of products was determined as follows. The reverse rate (i.e. either isobutene plus hydroperoxy-methyl radical or isobutenyl-hydroperoxide plus methyl radical) was likened to a methyl radical adding across the double bond in isobutene to yield neopentyl radical. The rate for this reaction was taken to be  $1.0 \times 10^{11} \exp(-11100/\text{RT})$ . Both forward rates, the  $\beta$ -scission reactions, were calculated using microscopic reversibility, Table 5.
3. In addition,  $\text{neo}\dot{\text{C}}_5\text{H}_{10}\text{OOH}$  radical can add to molecular oxygen to form hydroperoxy-neopentyl-peroxy ( $\text{neoC}_5\text{H}_{10}\text{OOH}-\dot{\text{O}}_2$ ) radical. The rate of this reaction was taken to be equal to that used for the addition of  $\text{O}_2$  to neopentyl radical.

In our earlier study [1] we included only H-atom isomerization on the  $\text{neoC}_5\text{H}_{10}\text{OOH}-\dot{\text{O}}_2$  radical from the carbon adjacent to the hydroperoxy group to form the stable 2-methyl isopropanal-2-methylhydroperoxide species and hydroxyl radical. This isomerization is included in this study, but we first create the radical precursor ( $\text{neo}\dot{\text{C}}_5\text{H}_9\text{q}_{2-\text{n}}$ ), reaction (1325), which decomposes to form 2-methyl isopropanal-2-methylhydroperoxide and hydroxyl radical, reaction (1852), Fig. 2. Moreover, we also include the possibility of H-atom abstraction from one of the two methyl groups adjacent to the hydroperoxy group to form the  $\text{neo}\dot{\text{C}}_5\text{H}_9\text{q}_2$  radical, reaction (1849), Fig. 2. The rate expressions for the two isomerizations, reactions

(1325) and (1849) are based on our calculations of all  $\text{R}\dot{\text{O}}_2 \rightleftharpoons \dot{\text{Q}}\text{OOH}$  isomerization reactions [21]. The  $\text{neo}\dot{\text{C}}_5\text{H}_9\text{O}_2$  radical can then decompose to form isobutenyl-hydroperoxide, formaldehyde and hydroxyl radical, reaction (1850), with the rate of this reaction estimated in the reverse direction, similar to reaction (1323) as described above.

Once the 2-methyl isopropanal-2-methylhydroperoxide species is formed we no longer allow it to decompose directly to 2-methylpropanal-2-yl ( $\text{t}\dot{\text{C}}_3\text{H}_6\text{CHO}$ ) radical, formaldehyde and hydroperoxy radical. (In our previous work [1] 2-methylpropanal-2-yl was named  $\text{iC}_3\text{H}_6\text{CHO}$ ). Currently, 2-methyl isopropanal-2-methylhydroperoxide undergoes O–O homolysis to generate 2-methyl isopropanal-2-methoxy and hydroxyl radicals, reaction (1434). The rate of reaction (1434) is based on the recommendations of Sahetchian et al. [36] for various molecular hydroperoxide pyrolyses. The  $\text{neoC}_5\text{ketox}$  radical so produced can then decompose to produce 2-methylpropanal-2-yl radical and formaldehyde, reaction (1846) or isomerize to generate the  $\text{neoC}_5\text{kejol}$  radical, reaction (1847), which can then decompose to form carbon monoxide and 1-propanol-2-methyl-2-yl radical, reaction (1848). The rate expression for reaction (1846) was estimated in the reverse (exothermic) direction, the addition of  $\text{t}\dot{\text{C}}_3\text{H}_6\text{CHO}$  to  $\text{CH}_2\text{O}$ , with the forward decomposition calculated from thermochemistry. This rate constant for the addition reaction was estimated to be  $1.0 \times 10^{11} \exp(-11.9 \text{ kcal/RT}) \text{ cm}^3 \text{ mol}^{-1} \text{ s}^{-1}$ . The rate of reaction (1847) is based on our recommendations for all  $\text{R}\dot{\text{O}}_2 \rightleftharpoons \dot{\text{Q}}\text{OOH}$  isomerization reactions [21], with the  $\mathcal{A}$ -factors adjusted downwards. The rate constant expression for reaction (1848) of  $1.5 \times 10^{11} \exp(-4.8 \text{ kcal/RT}) \text{ cm}^3 \text{ mol}^{-1} \text{ s}^{-1}$ , is similar to that recommended by Tsang and Hampson [40] for ethyl addition to carbon monoxide.

Finally, the kinetics of the oxidation of the  $\text{t}\dot{\text{C}}_3\text{H}_6\text{CHO}$  radical have also been updated. Previously, we included a one-step reaction in which the 2-methylpropanal-2-yl radical reacted with molecular oxygen generating acetone, carbon monoxide and hydroxyl radical. We now include this reaction as a multi-step process in which  $\text{t}\dot{\text{C}}_3\text{H}_6\text{CHO}$  adds to  $\text{O}_2$  creating the alkyl-peroxy radical, reaction (1484), with the rate of this reaction taken to equal that for the addition of  $\text{O}_2$  to neopentyl radical. The  $\text{tC}_3\text{H}_6\dot{\text{O}}_2\text{CHO}$  radical isomerizes *via* a H-atom shift to produce two different hydroperoxy-alkyl radicals reaction (1485) and (1486), the rates of these reactions are calculated in the same way as all  $\text{R}\dot{\text{O}}_2 \rightleftharpoons \dot{\text{Q}}\text{OOH}$  isomerization reactions [21]. The  $\text{tC}_3\text{H}_6\text{O}_2\dot{\text{H}}\text{CO}$  radical decomposes to form acetone, carbon monoxide and hydroxyl radical, reaction (1488). The rate of this reaction was estimated in the reverse direction, the addition of carbon monoxide to  $\text{t}\dot{\text{C}}_3\text{H}_6\text{O}_2\text{H}$ . A rate constant of  $1.5 \times 10^{11} \exp(-4.8 \text{ kcal/RT}) \text{ cm}^3 \text{ mol}^{-1} \text{ s}^{-1}$ , similar to that recommended by Tsang and Hampson [40] for ethyl addition to carbon monoxide was used. The  $\text{i}\dot{\text{C}}_3\text{H}_5\text{O}_2\text{HCHO}$  radical produces methacrolein ( $\text{iC}_3\text{H}_5\text{CHO}$ ) and hydroperoxy radical, reaction (1487), Fig. 3. The rate expressions for reaction (1487) was also estimated in the reverse direction, the addition hydroperoxyl radical to methacrolein with a rate expression of  $2.23 \times 10^{11} \exp(-10.6 \text{ kcal/RT}) \text{ cm}^3 \text{ mol}^{-1} \text{ s}^{-1}$ . The rate expressions for all of the above reactions are provided in Table 5.

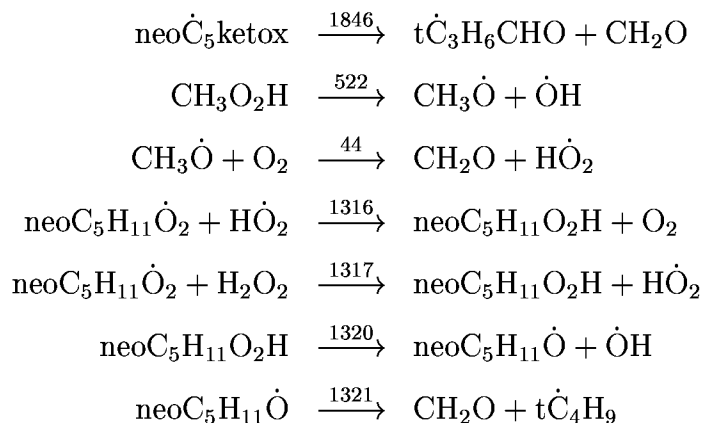
## Results and Discussion

In this section, the product species concentrations calculated by the model and measured in the experiment are discussed and compared. The product species results of the model

and the experiment are shown in Figs. 5-8. The species mole fractions are plotted versus the temperature at 200 ms which is the residence time at which the temperature and species mole fractions were measured experimentally. All temperatures below refer to the temperature at 200 ms residence time. Overall, there is very good agreement with both the experimental fuel decomposition and product species formation being reproduced by the model. At lower temperatures (620–650 K) formic acid is not predicted to be formed by the model although it is experimentally observed to peak at 645 K. The model predicts no reaction until the temperature reaches 630 K. We have included a formic acid production pathway from formaldehyde but we assume that there must be another formation pathway that we are unaware of. In addition, we have used the output edits from HCT to analyze the main flux through neopentane oxidation pathway. In Figs. 2 and 3 we have normalized the formation of neopentyl radical from neopentane to be 100%. The percentage numbers associated with each subsequent reaction is its contribution to the overall oxidation pathway at 757 K, where 27.9% of the fuel has been consumed at a residence time of 200 ms. We discuss below these main pathways producing the intermediate product species at 690 and 757 K as these are the two temperatures for which there are experimental species profiles versus time.

At both 690 and 757 K the main intermediate products formed are formaldehyde ( $\text{CH}_2\text{O}$ ), acetone ( $\text{CH}_3\text{COCH}_3$ ), isobutene ( $\text{iC}_4\text{H}_8$ ), 3,3-dimethyloxetane ( $\text{neoC}_5\text{H}_{10}\text{O}$ ), formic acid ( $\text{HCOOH}$ ), methacrolein ( $\text{iC}_3\text{H}_5\text{CHO}$ ), Fig 5, carbon monoxide and water, Fig. 6.

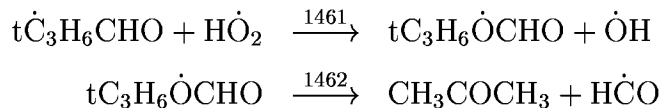
At 690 K formaldehyde is formed in almost equal quantities from the  $\beta$ -scission of the  $\text{neoC}_5\text{ketox}$  radical and the reaction of  $\text{CH}_3\dot{\text{O}}$  radical with  $\text{O}_2$ . About half as much is formed from the  $\beta$ -scission of  $\text{neoC}_5\text{H}_{11}\dot{\text{O}}$  radical. Both formaldehyde and acetone are formed from the decomposition of the  $\text{HO}_2\text{C}_4\text{H}_8\dot{\text{O}}$  radical, produced from the  $\text{iC}_4\text{H}_8\text{OH}$  radical as part of the Waddington mechanism [41, 42], Fig. 4.



At 757 K all of the above reactions still contribute to formaldehyde formation but the relative contribution from methyl-hydroperoxide is half that observed at 690 K.

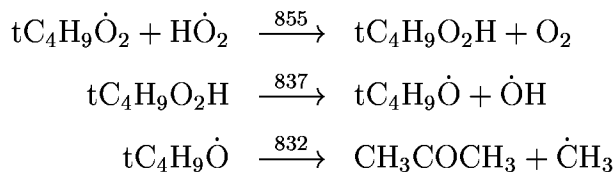
At both 690 and 757 K about twice as much acetone is formed from the oxidation the  $\text{tC}_3\text{H}_6\text{CHO}$  radical produced in reaction (1846) shown above than is produced from the  $\text{iC}_4\text{H}_8\text{OH}$  radical. The  $\text{tC}_3\text{H}_6\text{CHO}$  radical adds to molecular oxygen, and the resultant alkyl-peroxy radical undergoes internal H-atom isomerization to produce  $\text{tC}_3\text{H}_6\text{O}_2\text{H}\dot{\text{C}}\text{O}$  radical. This species decomposes to yield acetone, carbon monoxide and hydroxyl radical, Fig. 3.

The  $t\dot{C}_3H_6CHO$  radical can also form acetone through the following sequence of reactions:

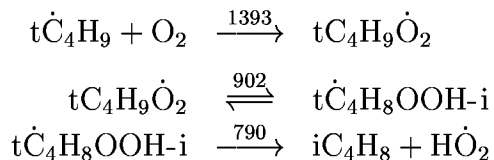


The contribution from this sequence is about a third that produced from the  $i\dot{C}_4H_8OH$  radical.

Finally, at 690 K the same quantity of acetone produced from the  $tC_3H_6\dot{O}CHO$  radical is also generated from the decomposition of the tert-butyl-alkoxy radical. This species is formed by the reaction of tert-butylperoxy radical with hydroperoxy radicals by analogy with the neopentyl-peroxy radical above, (reaction 1316).

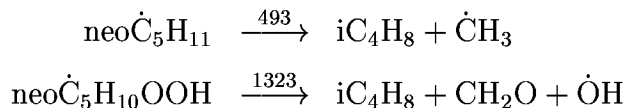


At 690 K isobutene is formed mainly through the oxidation of tert-butyl radicals, which are generated by the  $\beta$ -scission of neopentoxy radicals, reaction (1321). The reaction of  $neoC_5H_{11}\dot{O}_2$  radical with  $H\dot{O}_2$  and  $H_2O_2$  accounts for 18.7% of the total flux through the system at 690 K and reduces to 4% at 757 K. The tert-butyl radicals add to molecular oxygen to form tert-butylperoxy radical which can undergo an internal H-atom isomerization to generate the tert-hydroperoxy- iso-butyl radical,  $t\dot{C}_4H_8OOH-i$ . This then undergoes  $\beta$ -scission to generate isobutene and hydroperoxy radical.

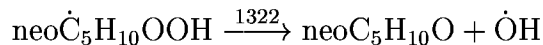


It is interesting that at 690 K the concentrations of isobutene and acetone are sensitive to the rate of tert-butylperoxy radical isomerization, reaction (902), and to its rate of reaction with hydroperoxy radical, reaction (855). At 690 K increasing the rate of reaction (902) produces more isobutene and reduces the concentration of acetone.

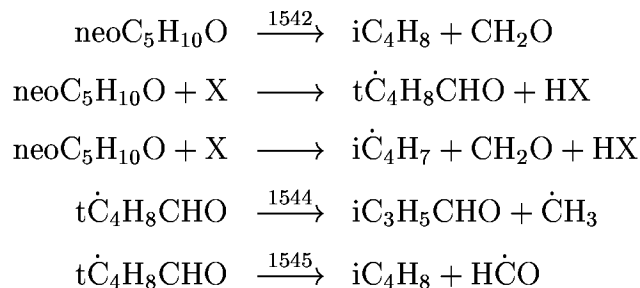
At 757 K almost twice as much isobutene is generated from  $\beta$ -scission of the neopentyl radical than from the oxidation of tert-butyl radical. In addition,  $\beta$ -scission of hydroperoxy-neopentyl radical produces almost equal quantities of isobutene as the tert-butyl pathway.



The formation of 3,3-dimethyloxetane can be explained exclusively by the reaction:

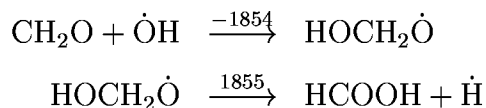


Included in the mechanism are the consumption reactions of neoC<sub>5</sub>H<sub>10</sub>O:

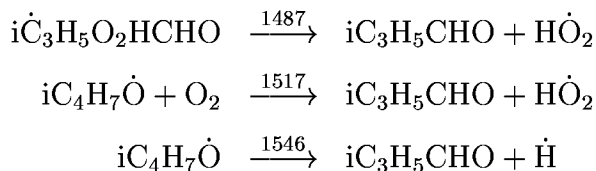


Radical species,  $\dot{\text{O}}\text{H}$  and  $\text{H}\dot{\text{O}}_2$  can abstract a H atom from either of two sites on neoC<sub>5</sub>H<sub>10</sub>O; from a secondary H atom bonded to the carbon which is part of the ring or from a primary H atom bonded to a methyl group. The more easily abstracted H atom is that bonded to the carbon in the ring structure, as this carbon atom is bonded to an oxygen atom which is electron withdrawing, and thus lowers the strength of the C—H bond. H atom abstraction is followed by ring opening yielding the t $\dot{\text{C}}_4\text{H}_8\text{CHO}$  radical. This t $\dot{\text{C}}_4\text{H}_8\text{CHO}$  radical subsequently undergoes  $\beta$ -scission leading to the formation of isobutene and formyl radical or methacrolein and methyl radical.

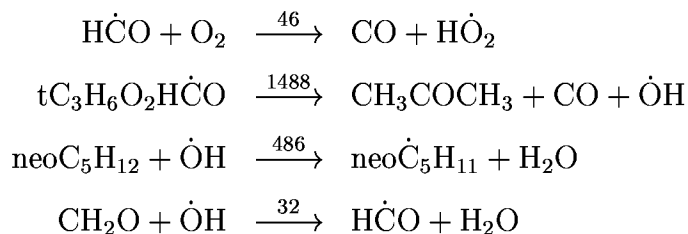
As stated earlier, formic acid is not well predicted in the temperature range 620–650 K. Above 650 K formic acid is predicted to be formed by hydroxyl radical addition to formaldehyde.



At both 690 and 757 K, methacrolein is mainly formed from the decomposition of the i $\dot{\text{C}}_3\text{H}_5\text{O}_2\text{HCHO}$  radical, reaction (1487). The oxidation and  $\beta$ -scission of methallyl-oxy radical, reactions (1717) and (1546) respectively, also produce methacrolein but are of relatively minor importance.



Carbon monoxide is formed from many reaction channels but mainly through the reaction of formyl radicals with molecular oxygen and the  $\beta$ -scission of the tC<sub>3</sub>H<sub>6</sub>O<sub>2</sub>H $\dot{\text{C}}\text{O}$  radical. Water is formed mainly by reaction of hydroxyl radicals with the fuel and with formaldehyde.

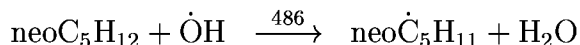


## Sensitivity Analysis

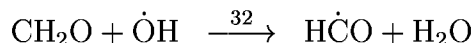
A detailed analysis was carried out to investigate the sensitivity of various reactions to the oxidation of neopentane. We used the flux diagram analysis in Fig. 2 as a basis in identifying the major oxidation pathways and thus the reactions responsible for neopentane oxidation. In addition, we also included sensitivity to other reactions such as  $\text{H}_2\text{O}_2 + \text{M} = \dot{\text{O}}\text{H} + \dot{\text{O}}\text{H} + \text{M}$ .

Sensitivity analyses were performed by multiplying the rate constant of a reaction by a factor of two (both forward and reverse rates) and then calculating the percent change in neopentane conversion. Analyses were performed using a residence time of 200 ms at two initial reaction temperatures of 675 K and 748 K, which resulted in outlet sampling temperatures of 690 K and 757 K, with respective fuel conversion of 32.0% and 26.9%. We define the sensitivity coefficient as the change in fuel conversion compared with the baseline simulation and express this as a percentage. Fuel conversion is a good measure of overall reactivity. A positive percent change indicates an increased level of fuel conversion while a negative change indicates a decreased level of fuel conversion. The reaction rate constants that exhibited the highest sensitivity are shown in Fig. 9. Reactions in which we multiplied both forward and reverse rate constants by a factor of two are denoted with an equal to “=” sign between reactants and products and reactions in which we multiplied only the forward rate constant (i.e. effected a change in the equilibrium constant) are denoted with an arrow “ $\Rightarrow$ ” between reactants and products.

The reaction with the highest positive sensitivity, and is therefore the most effective in promoting the overall rate of oxidation is reaction (486), H atom abstraction from neopentane by hydroxyl radical:

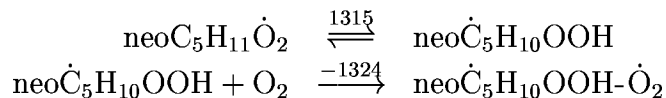


Conversely, the reaction with the highest negative sensitivity is H atom abstraction from formaldehyde by hydroxyl radical, reaction (32).



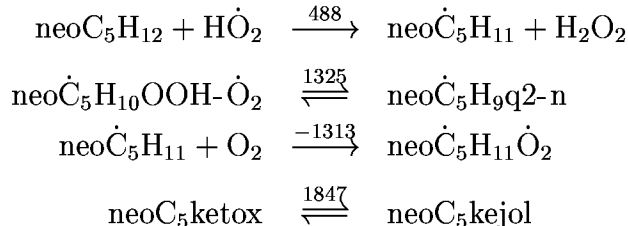
At both 690 and 757 K hydroxyl radicals react with neopentane and formaldehyde at much the same rate. Reaction (486) is the controlling step, producing neopentyl radicals which can add to molecular oxygen and proceed to branching as outlined in Fig. 2. The competing reaction with formaldehyde inhibits the production of neopentyl radicals and ultimately the amount of chain branching.

The second and third highest positive sensitivity coefficients are exhibited by the equilibrium constants associated with the neopentyl-peroxy radical isomerization, reaction (1315), and the addition of the subsequent hydroperoxy-neopentyl radical to molecular oxygen, reaction (1324).

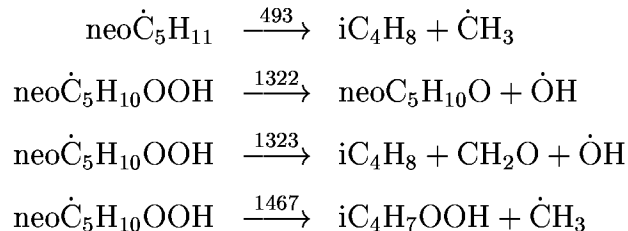


Multiplying both forward and reverse rate constants of reactions (1315) and (1324) by a factor of two also results in high positive sensitivity coefficients. Increasing the rates of these reactions increases the rate of hydroxyl radical production from chain branching, Fig. 2.

Other reactions showing positive sensitivity coefficients were H atom abstraction from the fuel by hydroperoxyl radical, reaction (488), the abstraction the isomerization of the hydroperoxy-neopentylperoxy radical, reaction (1325), the addition of neopentyl radical to molecular oxygen, reaction (1313), and isomerization of the 2-methyl isopropanal-2-methoxy radical to 3-hydroxy-2,2-dimethyl-propanal radical, reaction (1847).



Increasing the rates of reactions (1325), (1313) and (1847) promotes chain branching and so leads to the observed positive sensitivity coefficient. The  $\beta$ -scission of the hydroperoxy-neopentyl radical, reactions (1323) and (1467), and its rearrangement to form 3,3-dimethyloxetane and hydroxyl radical, reaction (1322), all show negative sensitivity coefficients as they compete with the above chain branching pathways. The  $\beta$ -scission of neopentyl radical, reaction (493), results in a negative sensitivity coefficient as this reaction competes with addition to molecular oxygen producing stable isobutene and relatively unreactive methyl radical.



The retarding influence of the last four aforementioned reactions slows the oxidation rate of neopentane and produces its observed NTC behavior. This explanation contrasts with other hydrocarbons where the formation of a conjugate olefin is the key retarding step that slows the oxidation rate of the hydrocarbon and produces its NTC behavior. Due to the molecular structure of neopentane, it does not produce a conjugate olefin, and its NTC behavior is due to the alternative four reactions above.

Another example of this competing positive/negative sensitivity coefficient is the isomerization of the  $\text{tC}_3\text{H}_6\dot{\text{O}}_2\text{CHO}$  which can form  $\text{tC}_3\text{H}_6\text{O}_2\text{H}\dot{\text{C}}\text{O}$  radical, reaction (1486), with subsequent decomposition forming a reactive hydroxyl radical resulting in a positive sensitivity coefficient. Alternatively, isomerization to form  $\text{iC}_3\text{H}_5\text{O}_2\text{HCHO}$  radical, reaction (1485), leads to less reactive hydroperoxyl radical and thus a negative sensitivity coefficient, Fig. 3.

The self reactions of hydroperoxyl radicals, reactions (50) and (518), and the reaction of hydrogen peroxide with hydroxyl radical, reaction (13), show negative sensitivity coefficients as hydroxyl radical reacts with hydrogen peroxide rather than with the fuel, creating hydroperoxyl radical and water. These two sets of reactions also have the same absolute values because doubling the rates of reactions (50) and (518) doubles the concentration of hydrogen peroxide and effectively doubles the rate of reaction (13).

Finally, the decomposition of hydrogen peroxide to form two reactive hydroxyl radicals, reaction (51), shows no sensitivity at 690 K but significant positive sensitivity at 757 K. Koert *et al.* [43] have observed a high sensitivity to this reaction. They found that this reaction is important in controlling the overall reaction rate at the end of the NTC region, and has comparatively little effect at the onset of the NTC region, which is exactly the behavior we observe in this study. It is also interesting to note that we observed no sensitivity to the reaction of fuel with molecular oxygen, the initiation reaction, at either 690 or 757 K.

## Conclusions

A detailed chemical kinetic model, which was developed previously [1], has been used as a basis for the current modeling of lean neopentane oxidation in a flow reactor. The earlier mechanism has been modified to include thermodynamic parameters of alkyl radical and alkyl-peroxy radical species based on the recent publications of Lay and Bozzelli [24] and Knyazev and Slagle [25]. In addition, an alternative isomerization reaction of the hydroperoxy neopentyl-peroxy ( $\text{neoC}_5\text{H}_{10}\text{OOH}\cdot\dot{\text{O}}_2$ ) radical has been added as has a two-step decomposition of the resultant dihydroperoxy-neopentyl-radical to form 2-methyl isopropanal-2-methylhydroperoxide. Moreover, the addition of 2-methylpropanal-2-yl ( $\text{tC}_3\text{H}_6\text{CHO}$ ) radical to molecular oxygen, with subsequent isomerization and decomposition to yield acetone, carbon monoxide and hydroxy radical is no longer treated as a one-step process. We have added a multi-step reaction sequence consistent with our current understanding of this type of reaction process.

Calculations on a limited set of experimental results have shown that the model can predict product formation with a high degree of accuracy. The overall reactivity of neopentane oxidation is reproduced very well by the model. Experiments indicate that neopentane does show negative temperature coefficient behavior similar to other alkanes, though it is not as pronounced as that shown by n-pentane for example. Since neopentane does not have a conjugate olefin, alternative explanations of its observed NTC behavior were sought. Modeling results indicate that this NTC behavior is caused by the  $\beta$ -scission of the neopentyl radical, reaction (493) and the chain propagation reactions of the hydroperoxyl-neopentyl radical, reactions (1322), (1323) and (1467).

## Acknowledgement

Henry Curran would like to acknowledge communications and discussions with Dr. Chris Morley which have encouraged a more detailed modeling analysis. The modeling analysis was supported by the Office of Basic Energy Sciences and was performed under the auspices of the U.S. Department of Energy at Lawrence Livermore National Laboratory under contract No. W-7405-ENG-48. The experimental work was supported by the Army Research Office under grant No. DAAH04-93-G-0042, No. DAAG55-98-1-0286 and No. DAAG55-97-1-0196.

## References

- [1] Curran, H. J., Pitz, W. J., Westbrook, C. K., Hisham, M. W. M. and Walker, R. W., *Twenty-Sixth Symposium (International) on Combustion*, The Combustion Institute, Pittsburgh, 1996, pp. 641–649.
- [2] Wang, S., Khan, A. R., Miller, D. L., and Cernansky, N. P., The Western States Section of The Combustion Institute, WSSCI 98S-61, (1998).
- [3] Cernansky, N. P., Green, R. M., Pitz, W. J., and Westbrook, C. K., *Combust. Sci. Tech.* 50:3–25 (1986).
- [4] Cox, A., Griffiths, J. F., Mohamed, C., Curran, H., Pitz, W. and Westbrook, C. *Twenty-Sixth Symposium (International) on Combustion*, The Combustion Institute, Pittsburgh, 1996, pp. 2685–2692.
- [5] Green, R. M., Cernansky, N. P., Pitz, W. J., and Westbrook, C. K., Society of Automotive Engineers publication, SAE-872108 (1987).
- [6] Fish, A., *Combust. Flame* 14:23–32 (1969).
- [7] Drysdale, D. D. and Norrish, R. G. W. *Proc. Roy. Soc.* A308, 305–325 (1969).
- [8] Baker, R. R., Baldwin, R. R. and Walker, R. W., *Combust. Flame* 14:31–36 (1970).
- [9] Baker, R. R., Baldwin, R. R., Everett, C. J. and Walker, R. W., *Combust. Flame* 25:285–300 (1975).
- [10] Baker, R. R., Baldwin, R. R. and Walker, R. W., *Combust. Flame* 27:147–161 (1976).
- [11] Antonik, S. and Lucquin, M., *Bull. Soc. Chim.*, 2796, (1968).
- [12] Koert, D. N. and Cernansky, N. P., *Meas. Sci. Tech.*, 3:607, (1992).
- [13] Koert, D. N., Miller, D. L., and Cernansky, N. P., *Energy and Fuels*, 6:485, (1992).
- [14] Hanna, A., Marshall, J. C. and Isenhour, T. L., *J. Chrom. Sci.* 17:434 (1979).
- [15] Lowry, S. R. and Huppler, D. A., *Anal. Chem.* 53:889 (1981).
- [16] 2. Olson, M. L., Proceedings of 1981 International FTIR Conference, (SPIE, 1981).
- [17] 3. Griffiths, P. R. and de Haseth, J. A., In *Fourier Transform Infrared Spectrometry*, John Wiley, New York, 1986, p. 607.
- [18] Wood, C. H., M. S. Thesis, Drexel University, Philadelphia, PA (1994).
- [19] Lund, C. M. and Chase, L., “HCT - A General Computer Program for Calculating Time-Dependent Phenomena Involving One-Dimensional Hydrodynamics, Transport, and Detailed Chemical Kinetics,” Lawrence Livermore National Laboratory report UCRL-52504, revised 1995.
- [20] Westbrook, C. K., and Pitz, W. J., The Western States Section of The Combustion Institute, WSSCI 93-011, (1993).
- [21] Curran, H. J., Gaffuri, P., Pitz, W. J., Westbrook, C. K., *Combust. and Flame*, 114:149–177 (1998).
- [22] Ritter, E. R. and Bozzelli, J. W., *Int. J. Chem. Kinet.* 23:767 (1991).
- [23] Lay, T. and Bozzelli, J. W., Chemical and Physical Processes in Combustion, The Eastern States Section of the Combustion Institute, Paper # 100 (1-4), (1993).
- [24] Lay, T. and Bozzelli, J. W., *J. Phys. Chem. A* 101:9505–9510 (1997).
- [25] Knyazev, V. D. and Slagle, I. R., *J. Phys. Chem. A* 102:1770–1778 (1998).

- [26] Slagle, I. R., Batt, L, Gmurczyk, G. W., Gutman, D. and Tsang, W., *J. Phys. Chem.* 95:7732–7739 (1991).
- [27] NIST Standard Reference Database 25: NIST Structures and Properties Version 2.0, software by Stephen E. Stein, Sharon G. Lias, Joel F. Liebman, Rhonda D. Levin, and Sherif A. Kafafi, 1994.
- [28] Cox, R. A. and Cole, J. A., *Combust. Flame* 60:109–123 (1985).
- [29] Morley, C., *Combust. Sci. Tech.* 55:115 (1987).
- [30] Compton, R. G., Hancock, G. and Pilling, M. J., *Chemical Kinetics*. Elsevier Science B. V., ISBN: 0-444-82485-5 (Vol. 35) 1997.
- [31] Xi, Z., Han, W-J and Bayes, K. D., *J. Phys. Chem.* 92:3450 (1988).
- [32] Hughes, K. J., Lightfoot, P. D. and Pilling, M. J., *Chem. Phys. Lett.* 191:581–586 (1992).
- [33] Hughes, K. J., Halford-Maw, P. A., Lightfoot, P. D., Turányi, T, and Pilling, M. J., *Twenty-Fourth Symposium (International) on Combustion.*, The Combustion Institute, Pittsburgh, 1992, pp. 645–652.
- [34] Baldwin, R. R., Hisham, M. W. M. and Walker, R. W., *J. Chem. Soc. Farad. Trans.* 1, 78:1615–1627 (1982).
- [35] Tsang, W., *J. Am. Chem. Soc.* 107:2872 (1985).
- [36] Sahetchian, K. A., Rigny, R, De Maleissye, J. T., Batt, L., Anwar Khan, M. and Mathews, S., *Twenty-Fourth Symposium (International) on Combustion*, The Combustion Institute, Pittsburgh, 1992, pp. 637–643.
- [37] Rowley, D. M., Lesclaux, R., Lightfoot, P. D., Hughes, K., Hurley, M. D., Rudy, S. and Wallington, T. J., *J. Phys. Chem.* 96:7043–7048 (1992).
- [38] Bozzelli, J. W. and Pitz, W. J. *Twenty Fifth Symposium (International) on Combustion*, The Combustion Institute, Pittsburgh, 1994, p. 783.
- [39] Pollard, R. T., *Comprehensive Chemical Kinetics*, (C. H. Bamford and C. F. H. Tipper, Eds), Elsevier, New York, 1977, Vol. 17, p. 249.
- [40] Tsang, W. and Hampson, R. F., *J. Phys. Chem. Ref. Data* 15:1087–1279 (1986).
- [41] Ray, D. J. M., Diaz, R. R. and Waddington, D. J., *Fourteenth Symposium (International) on Combustion.*, The Combustion Institute, Pittsburgh, 1973, p. 259.
- [42] Ray, D. J. M. and Waddington, D. J., *Combust. Flame* 20:327 (1973).
- [43] Koert, D., Pitz, W. J., Bozzelli J. W., and Cernansky, N. P., *Twenty-Sixth Symposium (International) on Combustion.*, The Combustion Institute, Pittsburgh, 1996, pp. 633–640.
- [44] Cohen, N., *Int. J. Chem. Kinet.* 23:397–417 (1991).

$\dot{R}$	$-\Delta H_{\text{rxn}}^{\circ}$ @ 298 K (kcal/mol)		$-\Delta S_{\text{rxn}}^{\circ}$ @ 298 K (cal/mol-K)	
	[25]	this study	[25]	this study
$\dot{C}H_3$	32.74	32.82	31.05	31.20
$\dot{C}_2H_5$	35.47	35.50	33.58	33.61
$i\dot{C}_3H_7$	37.14	37.22	37.26	37.44
$t\dot{C}_4H_9$	36.52	36.50	39.51	39.50
$neo\dot{C}_5H_{11}$	—	35.50	—	34.03

Table 1: Thermodynamic functions of  $\dot{R} + O_2 \rightleftharpoons R\dot{O}_2$  reactions.

$\dot{R}$	$H_f^{\circ}$ @ 298 K (kcal/mol)						
	$\dot{R}$		$R\dot{O}_2$		ROOH		
	[25]	this study	[25]	this study	[24]	[25]	this study
$\dot{C}H_3$	34.89	34.82	2.15	2.00	-31.80	-33.22	-31.80
$\dot{C}_2H_5$	28.92	28.60	-6.55	-6.90	-39.90	-41.92	-40.70
$i\dot{C}_3H_7$	21.51	21.02	-15.60	-16.20	-49.00	-51.00	-50.00
$t\dot{C}_4H_9$	12.26	11.90	-25.26	-24.60	-58.40	-59.63	-58.40

Table 2: Enthalpies of formation for selected species.

Species	H <sub>f</sub> <sup>o</sup> @ 298 K (kcal/mol)	S <sub>f</sub> <sup>o</sup> @ 298 K (cal/mol-K)	C <sub>p</sub> @ 300 K (cal/mol-K)
neoC <sub>5</sub> H <sub>12</sub>	-40.30	72.87	29.13
neoC <sub>5</sub> H <sub>11</sub>	8.70	79.46	28.54
neoC <sub>5</sub> H <sub>11</sub> O <sub>2</sub> H	-60.60	95.56	37.46
neoC <sub>5</sub> H <sub>11</sub> Ö <sub>2</sub>	-26.80	94.43	35.41
neoC <sub>5</sub> H <sub>10</sub> OOH	-11.60	101.16	36.69
neoC <sub>5</sub> H <sub>11</sub> OH	-76.10	86.27	32.23
neoC <sub>5</sub> H <sub>11</sub> Ö	-24.14	84.81	31.25
neoC <sub>5</sub> H <sub>10</sub> O	-33.33	77.84	26.40
neoC <sub>5</sub> OOH-O <sub>2</sub> H	-80.90	117.67	45.79
neoC <sub>5</sub> OOH-Ö <sub>2</sub>	-47.10	116.54	43.74
neoC <sub>5</sub> ket	-78.60	104.79	37.92
neoC <sub>5</sub> H <sub>9</sub> q <sub>2</sub>	-31.90	121.09	45.02
neoC <sub>5</sub> H <sub>9</sub> q <sub>2</sub> -n	-37.00	121.49	45.93
neoC <sub>5</sub> ketol	-94.10	95.50	32.69
neoC <sub>5</sub> ketox	-42.14	94.04	31.71
neoC <sub>5</sub> kejol	-57.20	96.62	31.86
iC <sub>3</sub> H <sub>6</sub> O <sub>2</sub> HCHO	-74.90	94.37	32.51
iC <sub>3</sub> H <sub>6</sub> Ö <sub>2</sub> CHO	-41.10	93.24	30.46
iC <sub>3</sub> H <sub>5</sub> O <sub>2</sub> HCHO	-25.90	97.94	31.86
tC <sub>3</sub> H <sub>6</sub> O <sub>2</sub> HÖ	-38.00	95.49	31.68

Table 3: Thermodynamic properties for selected species

T = 700 K	k <sub>493</sub> (s <sup>-1</sup> )	k <sub>1315</sub> (s <sup>-1</sup> )
This work	9.75 × 10 <sup>+03</sup>	2.71 × 10 <sup>+03</sup>
This work		9.43 × 10 <sup>+02</sup> <sup>a</sup>
Ref. [1]	8.92 × 10 <sup>+03</sup>	7.66 × 10 <sup>+04</sup>
Ref. [26]	1.78 × 10 <sup>+04</sup>	—
Ref. [32, 33]	1.56 × 10 <sup>+04</sup>	1.24 × 10 <sup>+03</sup>
Ref. [34]	1.39 × 10 <sup>+04</sup>	9.65 × 10 <sup>+02</sup> <sup>b</sup>
Ref. [35]	5.27 × 10 <sup>+03</sup>	—

Table 4: Comparison of current model rates with literature recommendations. <sup>a</sup> Overall *net* rate. <sup>b</sup> Rate constant corrected using currently accepted values of K<sub>-1313</sub>

	Reaction	$\mathcal{A}$	$n$	$\mathcal{E}_a$	Reference
486	$\text{neoC}_5\text{H}_{12} + \dot{\text{O}}\text{H} = \text{neoC}_5\text{H}_{11} + \text{H}_2\text{O}$	3.16E07	1.80	298.	[44]
493	$\text{neoC}_5\text{H}_{11} = \text{iC}_4\text{H}_8 + \dot{\text{C}}\text{H}_3$	3.06E17	-1.20	32290.	†
-1313	$\text{neoC}_5\text{H}_{11} + \text{O}_2 = \text{neoC}_5\text{H}_{11}\dot{\text{O}}_2$	1.99E17	-2.10	0.	[31]
1315	$\text{neoC}_5\text{H}_{11}\dot{\text{O}}_2 = \text{neoC}_5\text{H}_{10}\text{OOH}$	1.13E11	0.00	24400.	†
1322	$\text{neoC}_5\text{H}_{10}\text{OOH} = \text{neoC}_5\text{H}_{10}\text{O} + \text{OH}$	2.50E10	0.00	15250.	[1]
1323	$\text{neoC}_5\text{H}_{10}\text{OOH} = \text{iC}_4\text{H}_8 + \text{CH}_2\text{O} + \dot{\text{O}}\text{H}$	3.01E17	-1.17	29950.	†
1467	$\text{neoC}_5\text{H}_{10}\text{OOH} = \text{iC}_4\text{H}_7\text{OOH} + \dot{\text{C}}\text{H}_3$	2.79E17	-1.19	30610.	†
1316	$\text{neoC}_5\text{H}_{11}\dot{\text{O}}_2 + \text{H}\dot{\text{O}}_2 = \text{neoC}_5\text{H}_{11}\text{O}_2\text{H} + \text{O}_2$	1.75E10	0.00	-3275.	†
1317	$\text{neoC}_5\text{H}_{11}\dot{\text{O}}_2 + \text{H}_2\text{O}_2 = \text{neoC}_5\text{H}_{11}\text{O}_2\text{H} + \text{H}\dot{\text{O}}_2$	2.40E12	0.00	10000.	[1]
1320	$\text{neoC}_5\text{H}_{11}\text{O}_2\text{H} = \text{neoC}_5\text{H}_{11}\dot{\text{O}} + \dot{\text{O}}\text{H}$	1.50E16	0.00	42500.	†
-1324	$\text{neoC}_5\text{H}_{10}\text{OOH} + \text{O}_2 = \text{neoC}_5\text{H}_{10}\text{OOH}-\dot{\text{O}}_2$	1.99E17	-2.10	0.	†
1325	$\text{neoC}_5\text{H}_{10}\text{OOH}-\dot{\text{O}}_2 = \text{neoC}_5\text{H}_9\text{q}_2\text{-n}$	2.50E10	0.00	21400.	†
1849	$\text{neoC}_5\text{H}_{10}\text{OOH}-\dot{\text{O}}_2 = \text{neoC}_5\text{H}_9\text{q}_2$	7.50E10	0.00	24400.	†
1850	$\text{neoC}_5\text{H}_9\text{q}_2 = \text{iC}_4\text{H}_7\text{OOH} + \text{CH}_2\text{O} + \dot{\text{O}}\text{H}$	3.42E14	0.37	30920.	†
1851	$\text{neoC}_5\text{H}_9\text{q}_2 = \text{iC}_4\text{H}_6\text{q}_2\text{-ii} + \dot{\text{C}}\text{H}_3$	2.19E16	-0.71	32650.	†
1852	$\text{neoC}_5\text{H}_9\text{q}_2\text{-n} = \text{neoC}_5\text{ket} + \dot{\text{O}}\text{H}$	4.38E15	-2.10	5480.	†
1434	$\text{neoC}_5\text{ket} = \text{neoC}_5\text{ketox} + \dot{\text{O}}\text{H}$	1.50E16	0.00	42000.	†
1846	$\text{neoC}_5\text{ketox} = \text{tC}_3\text{H}_6\text{CHO} + \text{CH}_2\text{O}$	8.57E17	-1.59	11300.	†
1847	$\text{neoC}_5\text{ketox} = \text{neoC}_5\text{kejol}$	2.00E11	0.00	7600.	†
1848	$\text{neoC}_5\text{kejol} = \text{iC}_4\text{H}_8\text{OH} + \text{CO}$	2.27E21	-2.34	11020.	†
1484	$\text{tC}_3\text{H}_6\dot{\text{O}}_2\text{CHO} = \text{tC}_3\text{H}_6\text{CHO} + \text{O}_2$	2.79E25	-4.07	28450.	†
1485	$\text{tC}_3\text{H}_6\dot{\text{O}}_2\text{CHO} = \text{iC}_3\text{H}_5\text{O}_2\text{HCHO}$	6.00E11	0.00	29880.	†
1486	$\text{tC}_3\text{H}_6\dot{\text{O}}_2\text{CHO} = \text{tC}_3\text{H}_6\text{O}_2\text{H}\dot{\text{C}}\text{O}$	1.00E11	0.00	25750.	†
1487	$\text{iC}_3\text{H}_5\text{O}_2\text{HCHO} = \text{iC}_3\text{H}_5\text{CHO} + \text{H}\dot{\text{O}}_2$	8.94E20	-2.44	15030.	†
1488	$\text{tC}_3\text{H}_6\text{O}_2\text{H}\dot{\text{C}}\text{O} = \text{CH}_3\text{COCH}_3 + \text{CO} + \dot{\text{O}}\text{H}$	4.24E18	-1.43	4800.	†

Table 5: Rate expressions for critical reactions in neopentane oxidation;  $\text{cm}^3/\text{mol}/\text{sec}/\text{cal}$  units. †: *this study, see text.*

## Figure Captions

**Figure 1:** Reactivity mapping for neopentane at two different nitrogen dilutions and comparison with n-pentane reactivity,  $P = 8$  atm,  $\phi = 0.3$ . ● n-pentane 85%  $N_2$  dilution, ○ neopentane 75%  $N_2$  dilution, ★ neopentane 85%  $N_2$  dilution. Lines are model predicted CO concentrations.

**Figure 2:** Kinetic scheme for neopentane oxidation. Percentiles are the fraction of neopentane that proceeds through the relevant path based on the modeling results at 757 K and 8 atm. Numbers in parenthesis refer to the reaction number in the kinetic mechanism.

**Figure 3:** Oxidation of 2-methylpropanal-2-yl radical. Percentiles are the fraction of neopentane that proceeds through the relevant path based on the modeling results at 757 K and 8 atm. Numbers in parenthesis refer to the reaction number in the kinetic mechanism.

**Figure 4:** Formation of acetone and formaldehyde *via* the Waddington mechanism.

**Figure 5:** Neopentane Oxidation:  $T = 620\text{--}820$  K,  $P = 8$  atm,  $\phi = 0.3$ . ●  $CH_2O$ , ○  $CH_3COCH_3$ , ★  $iC_4H_8$ , ◇  $neoC_5H_{10}O$ , ×  $HCOOH$ , and △  $iC_3H_5CHO$ . Dotted lines correspond to open symbols. Species and temperatures reported at 200 ms.

**Figure 6:** Neopentane Oxidation:  $T = 620\text{--}820$  K,  $P = 8$  atm,  $\phi = 0.3$ . ●  $neoC_5H_{12}$ , ○  $H_2O$ , and ★  $CO$ . Dotted lines correspond to open symbols. Species and temperatures reported at 200 ms.

**Figure 7:** Neopentane Oxidation:  $T = 690$  K,  $P = 8$  atm,  $\phi = 0.3$ . ●  $CO$ , ○  $CH_2O$ , ★  $CH_3COCH_3$ , ◇  $iC_4H_8$ , ×  $HCOOH$ , □  $neoC_5H_{10}O$  and +  $iC_3H_5CHO$ . Dotted lines correspond to open symbols.

**Figure 8:** Neopentane Oxidation:  $T = 757$  K,  $P = 8$  atm,  $\phi = 0.3$ . ●  $CO$ , ○  $CH_2O$ , ★  $CH_3COCH_3$ , ◇  $iC_4H_8$ , ×  $neoC_5H_{10}O$ , □  $HCOOH$  and +  $iC_3H_5CHO$ . Dotted lines correspond to open symbols.

**Figure 9:** Sensitivity coefficients for neopentane oxidation. 0.197%  $neoC_5H_{12}$  and 94.5%  $N_2$  at 8 atm,  $\phi = 0.3$ ,  $\tau = 200$  ms. ( $Q = neo\dot{C}_5H_{10}$ ,  $R = neoC_5H_{11}$ ).

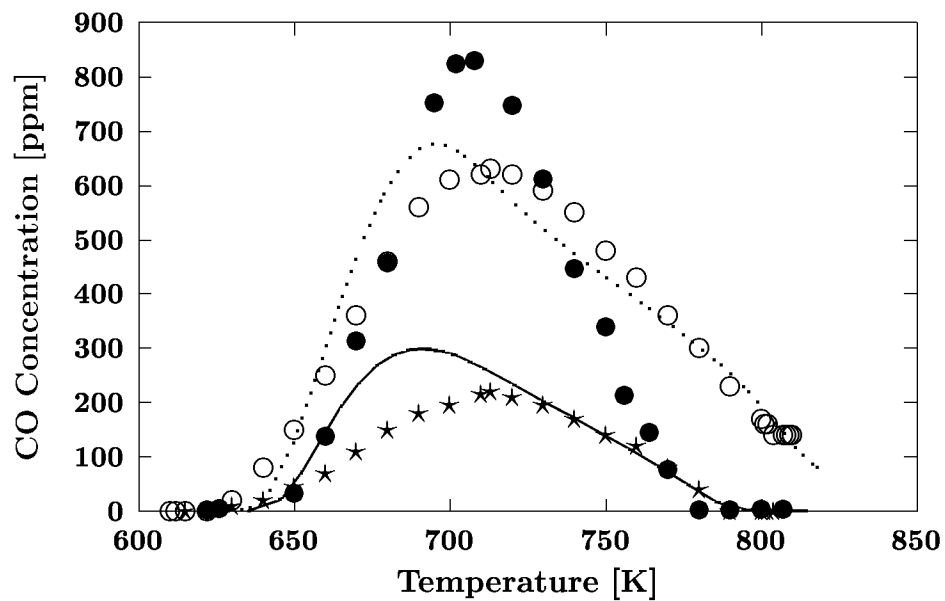


Figure 1: Reactivity mapping for neopentane at two different nitrogen dilutions and comparison with n-pentane reactivity,  $P = 8$  atm,  $\phi = 0.3$ .  $\bullet$  n-pentane 85%  $N_2$  dilution,  $\circ$  neopentane 75%  $N_2$  dilution,  $\star$  neopentane 85%  $N_2$  dilution. Lines are model predicted CO concentrations.

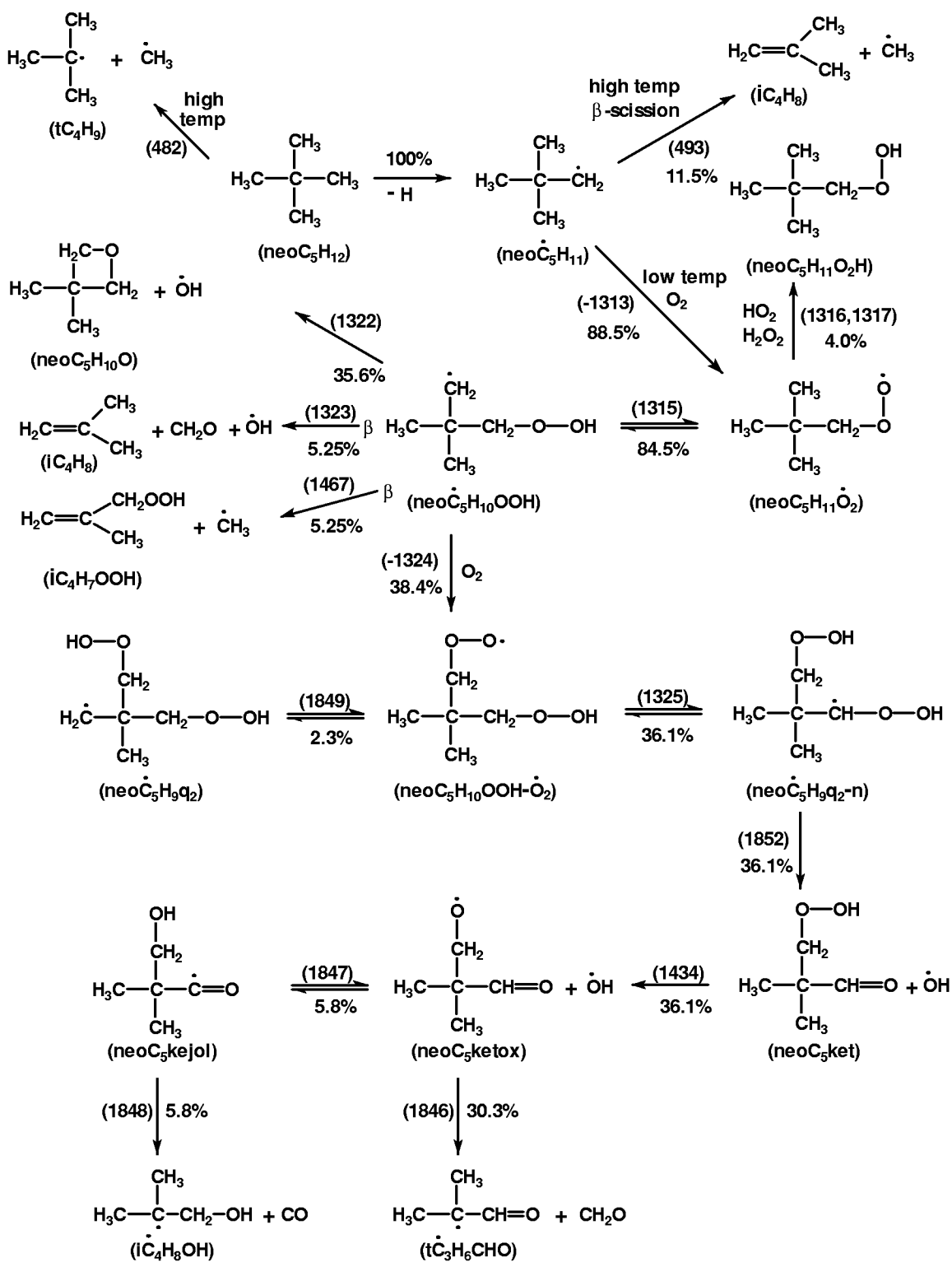


Figure 2: Kinetic scheme for neopentane oxidation. Percentiles are the fraction of neopentane that proceeds through the relevant path based on the modeling results at 757 K and 8 atm. Numbers in parenthesis refer to the reaction number in the kinetic mechanism.

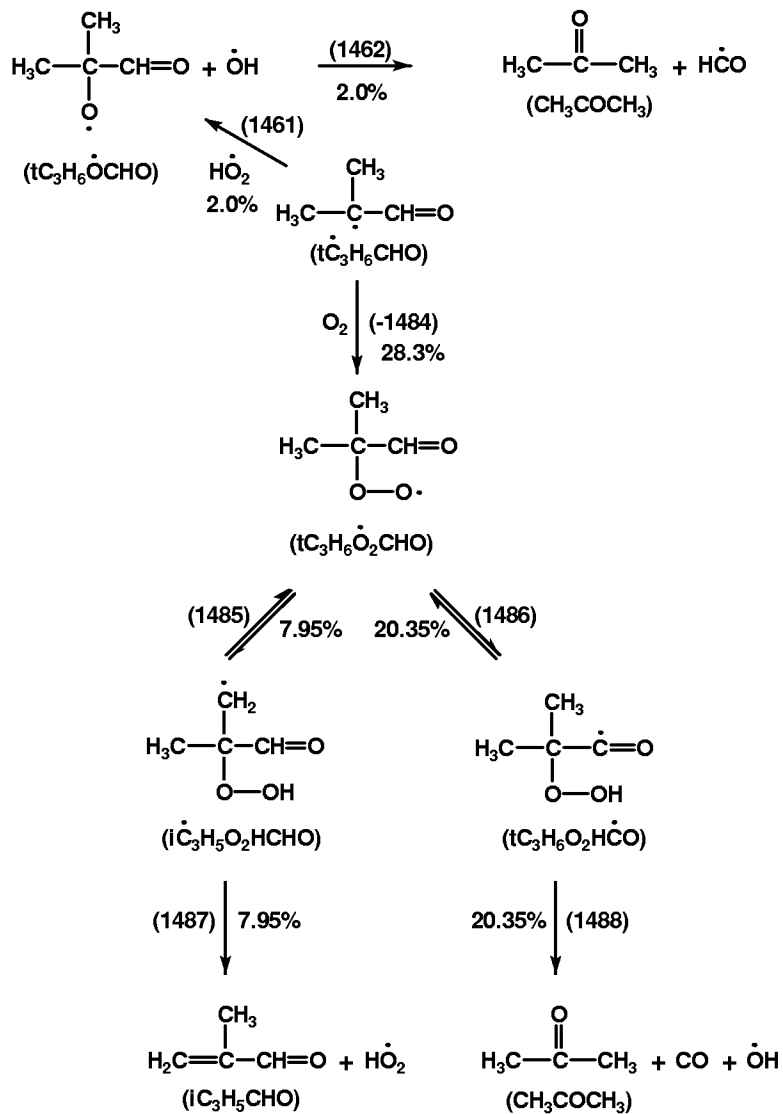


Figure 3: Oxidation of 2-methylpropanal-2-yl radical. Percentiles are the fraction of neopentane that proceeds through the relevant path based on the modeling results at 757 K and 8 atm. Numbers in parenthesis refer to the reaction number in the kinetic mechanism.

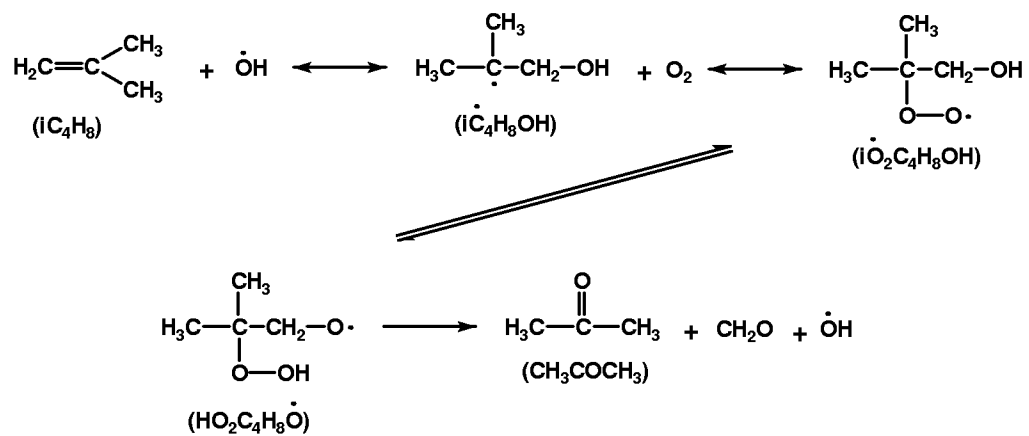


Figure 4: Formation of acetone and formaldehyde *via* the Waddington mechanism.

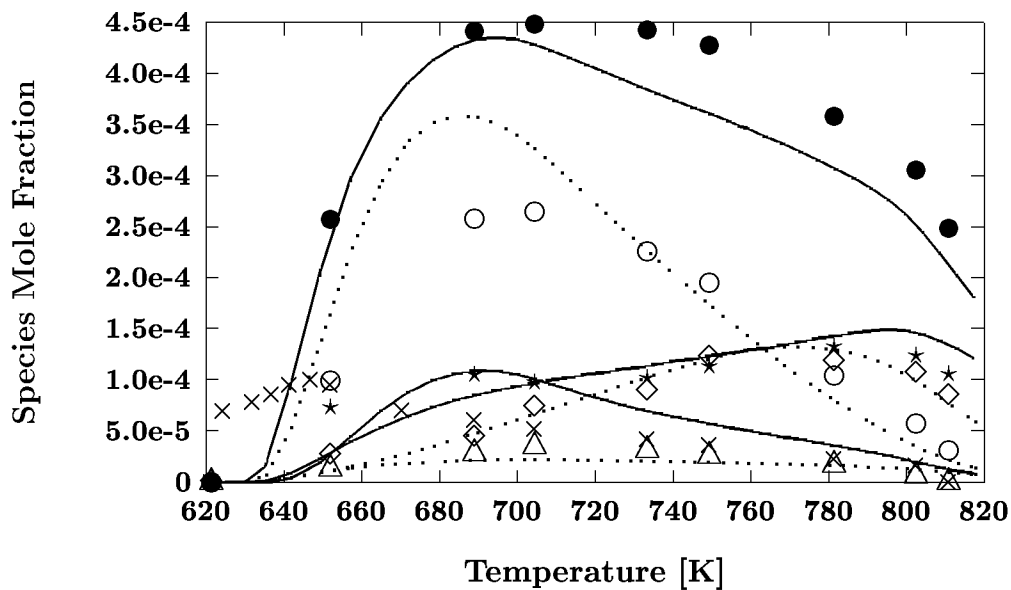


Figure 5: Neopentane Oxidation:  $T = 620\text{--}820$  K,  $P = 8$  atm,  $\phi = 0.3$ .  $\bullet$   $\text{CH}_2\text{O}$ ,  $\circ$   $\text{CH}_3\text{COCH}_3$ ,  $\star$   $\text{iC}_4\text{H}_8$ ,  $\diamond$   $\text{neoC}_5\text{H}_{10}\text{O}$ ,  $\times$   $\text{HCOOH}$ , and  $\triangle$   $\text{iC}_3\text{H}_5\text{CHO}$ . Dotted lines correspond to open symbols. Species and temperatures reported at 200 ms.

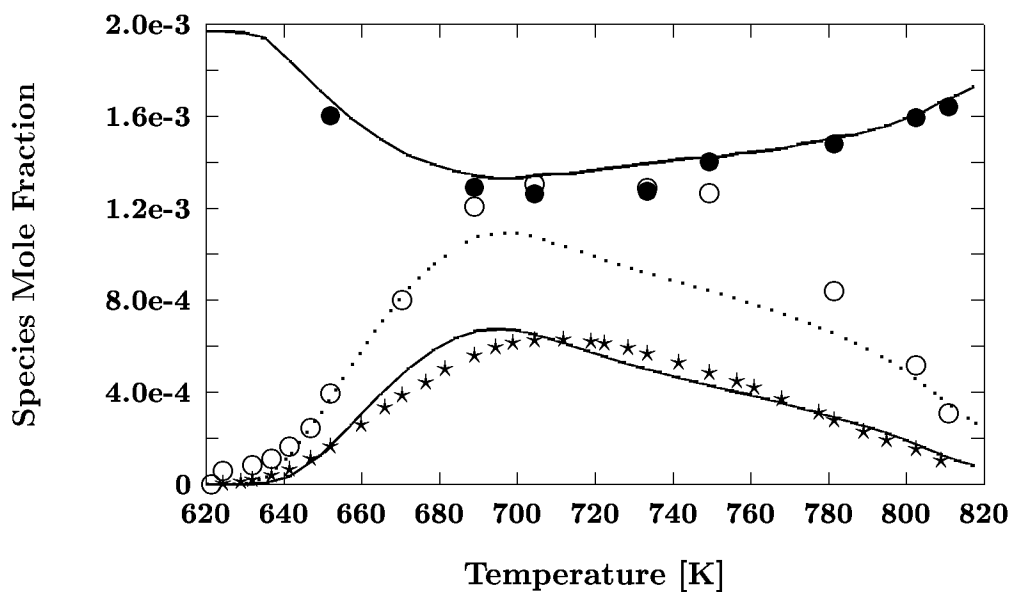


Figure 6: Neopentane Oxidation:  $T = 620\text{--}820$  K,  $P = 8$  atm,  $\phi = 0.3$ .  $\bullet$   $\text{neoC}_5\text{H}_{12}$ ,  $\circ$   $\text{H}_2\text{O}$ , and  $\star$   $\text{CO}$ . Dotted lines correspond to open symbols. Species and temperatures reported at 200 ms.

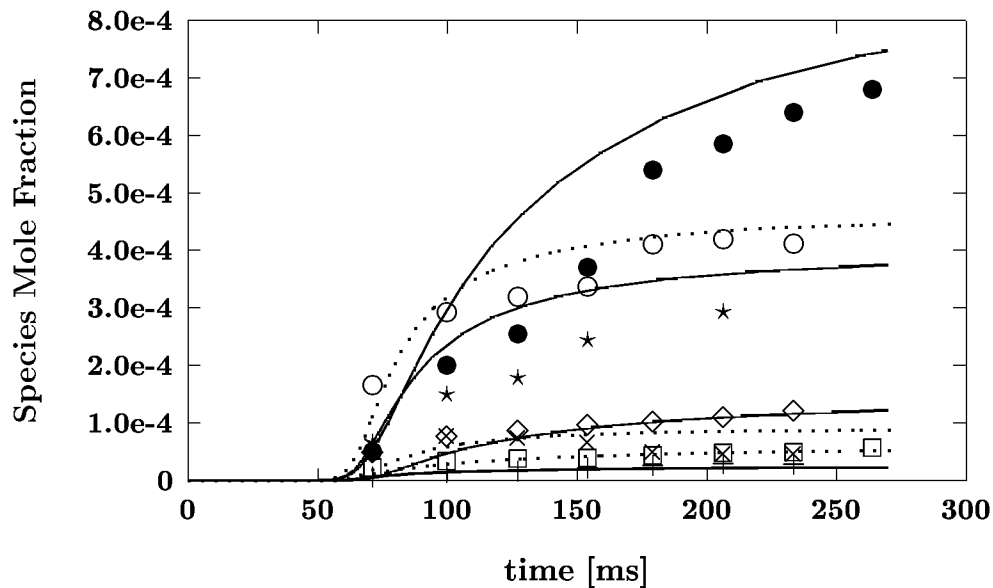


Figure 7: Neopentane Oxidation:  $T = 690$  K,  $P = 8$  atm,  $\phi = 0.3$ .  $\bullet$  CO,  $\circ$   $\text{CH}_2\text{O}$ ,  $\star$   $\text{CH}_3\text{COCH}_3$ ,  $\diamond$   $\text{iC}_4\text{H}_8$ ,  $\times$   $\text{HCOOH}$ ,  $\square$   $\text{neoC}_5\text{H}_{10}\text{O}$  and  $+$   $\text{iC}_3\text{H}_5\text{CHO}$ . Dotted lines correspond to open symbols.

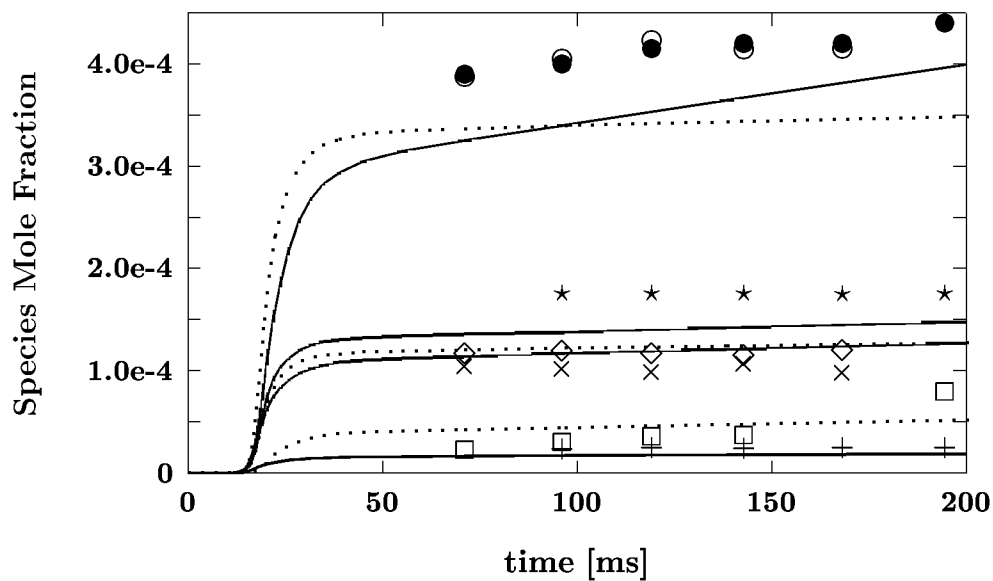


Figure 8: Neopentane Oxidation:  $T = 757$  K,  $P = 8$  atm,  $\phi = 0.3$ .  $\bullet$  CO,  $\circ$   $\text{CH}_2\text{O}$ ,  $\star$   $\text{CH}_3\text{COCH}_3$ ,  $\diamond$   $\text{iC}_4\text{H}_8$ ,  $\times$   $\text{neoC}_5\text{H}_{10}\text{O}$ ,  $\square$   $\text{HCOOH}$  and  $+$   $\text{iC}_3\text{H}_5\text{CHO}$ . Dotted lines correspond to open symbols.

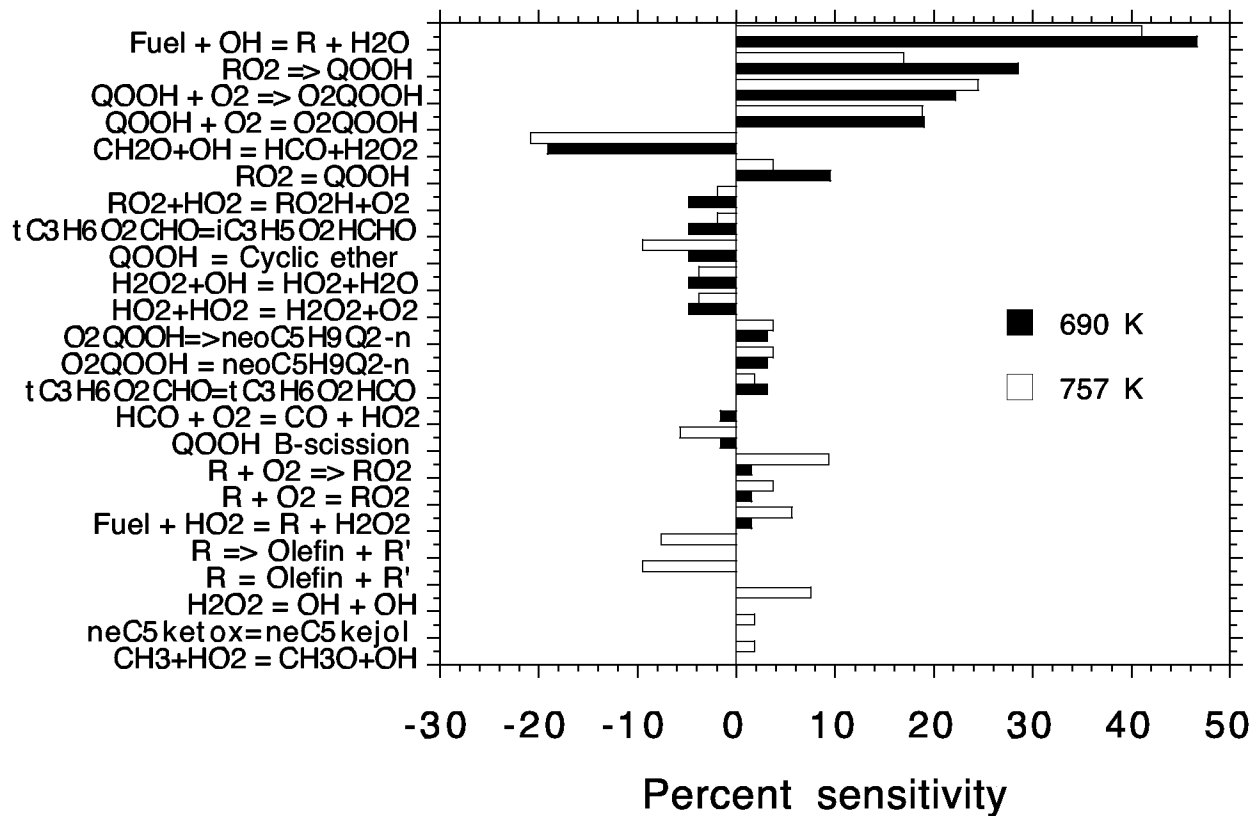


Figure 9: Sensitivity coefficients for neopentane oxidation. 0.197% neoC<sub>5</sub>H<sub>12</sub> and 94.5% N<sub>2</sub> at 8 atm,  $\phi = 0.3$ ,  $\tau = 200$  ms. (Q = neoC<sub>5</sub>H<sub>10</sub>, R = neoC<sub>5</sub>H<sub>11</sub>).